ROYAL SOCIETY
OF CHEMISTRY

PAPER

Check for updates

Perylene dye@SiO$_2$ core–shell nanoparticles with intense fluorescence†

Mark Rutschmann and Claus Feldmann ⓘD *

PD/CC@SiO$_2$ core–shell nanoparticles (PD: perylene dye, CC: cholecalciferol/vitamin D$_3$) were prepared using a water-based injection method. Specifically, a solution of the PD (fluorescent red (FR), fluorescent orange (FO), fluorescent yellow (FY)), CC, and octyltriethoxysilane (OTES) as a silica precursor in ethanol was injected in water at 70 °C and pH 5. The core–shell nanoparticles exhibited an outer particle diameter of 29 ± 11 nm and an inner core of 12 ± 4 nm. Suspensions (up to 10 mg mL^{-1}) were colloidally highly stable due to the negative surface charging (-40 to -50 mV). CC efficiently allowed disturbing of the π-stacking of the PD, such that, *e.g.*, FR/CC@SiO$_2$ nanoparticles with 10 wt% FR showed intense emission with quantum yields near unity (98%) and without any concentration quenching. In contrast to the freely-dissolved dyes, PD in the nanoparticle core did not show any photobleaching even after 20 hours of continuous UV illumination (280 nm). As proof-of-the-concept, suspensions and thin films were realised showing intense emission from red to yellow. Exemplarily, FR/CC@SiO$_2$ core–shell nanoparticles were examined in detail, including electron microscopy, element mapping, dynamic light scattering, infrared spectroscopy, elemental analysis, UV-Vis spectroscopy, and photoluminescence spectroscopy.

1. Introduction

Perylenes are generally known as photochemically and thermally most stable fluorescent dyes showing exceptionally high quantum yields of up to 100%.[1] Besides outstanding properties, such as intense emission, a variable wavelength of emission, excellent stability, and low costs, perylene-type dyes also have certain disadvantages. Thus, many perylene derivatives are lipophilic and predominately insoluble in water.[2] Moreover, the flat molecular appearance and the extended aromatic molecule backbone tend to involve considerable π-stacking in the solid state as well as at high concentrations in the solution. As a result, the fluorescence is often partially or even completely quenched.[3] Although highly stable in comparison to other organic dyes, finally, perylene-type dyes nevertheless show certain photobleaching over time, particularly if exposed to UV light (<350 nm) but also even for excitation at the wavelength of maximum dye absorption.[4]

To take advantage of the outstanding luminescence properties of perylene-type dyes in nanoparticles, for instance, as emissive biomarkers, for sensing, or as emissive polymers, they were embedded in polymer matrices,[5] silica,[6] carbon dots,[7] or

Institut für Anorganische Chemie, Karlsruhe Institute of Technology (KIT), Engesserstrasse 15, Karlsruhe 76131, Germany. E-mail: claus.feldmann@kit.edu; Fax: +49-721-60844892; Tel: +49-721-60842855

† Electronic supplementary information (ESI) available: Details regarding the analytical techniques and additional data related to material characterisation. See DOI: https://doi.org/10.1039/d2tc03981h

functionalised with sterically demanding groups.[8] Nevertheless, the concentration of the perylene dye is usually limited to $\leq 1\%$ of the total nanoparticle mass. Recently, perylene-loaded nanoparticles were also discussed as solar absorbers[9] as well as solar concentrators[10] in thin-film solar cells. For these applications, the nanoparticles are either non-luminescent or have quantum yields significantly below the values of the freely dissolved perylene molecules.

We present SiO$_2$ core–shell nanoparticles that were prepared by the injection of octyltriethoxysilane (OTES) and the perylene dye (PD) in a mixture of cholecalciferol (CC) and ethanol in water at 70 °C at a slightly acidic pH. The resulting PD/CC@SiO$_2$ core–shell nanoparticles contained 10 wt% of PD and exhibited quantum yields near unity similar to the freely dissolved perylene as well as long-term photostability. Due to the incorporation of fluorescent red (FR), fluorescent orange (FO), or fluorescent yellow (FY), the PD/CC@SiO$_2$ core–shell nanoparticles showed intense emission from red to yellow. The first conceptual studies also showed their suitability for printing and thin-film formation.

2. Experimental section

2.1. Synthesis

PD/CC@SiO$_2$ core–shell nanoparticles. 20 mg of cholecalciferol (CC, C$_{27}$H$_{44}$O, 0.05 mmol, Sigma-Aldrich, Germany) and 10 mg of perylene dye fluorescent red (FR), fluorescent orange (FO), fluorescent yellow (FY) (Kremer Pigments, Germany) were

This journal is © The Royal Society of Chemistry 2023

dissolved in a mixture of 1.0 mL of *n*-octyltriethoxysilane (OTES, $C_{14}H_{52}O_3Si$, 0.88 g, 3.18 mmol, Sigma-Aldrich) and 4 mL of ethanol (Sigma-Aldrich). Thereafter, this solution was injected under vigorous stirring into 50 mL of demineralised water at 70 °C, which was adjusted by adding 0.20 mL of 0.1 M HCl to pH 5 prior to the injection (pH measured with a pH electrode). After 8 h of continuous heating and stirring, 0.25 mL of 13.3 M ammonia solution was added to adjust the pH to 8. After an additional 18 h of heating and stirring, the suspension was naturally cooled to room temperature. The obtained suspension was concentrated by centrifugation (45 000 × *g*, 15 min). Since the density of the PD/CC@SiO$_2$ core–shell nanoparticles was lower than that of water, the bottom phase was removed with a syringe (Fig. S1, ESI†). Thereafter, demineralised water was again added, the suspension was intensely mixed, and the purification process was repeated twice to remove all salts and excess starting materials. The resulting PD@SiO$_2$ core–shell nanoparticle suspension was colloidally highly stable and used as follows with a concentration of 10 mg mL^{-1}. Higher nanoparticle concentrations lead to the formation of highly viscous gel-like suspensions. The as-prepared PD@SiO$_2$ nanoparticle suspensions were intensely coloured and showed intense fluorescence even under daylight.

2.2. Characterisation

Details related to the analytical equipment and the sample preparation for characterisation are described in the ESI.†

3. Results and discussion

3.1 Synthesis of PR/CC@SiO$_2$ core–shell nanoparticles

PD/CC@SiO$_2$ core–shell nanoparticles were prepared *via* an injection-driven synthesis strategy (Fig. 1).[11] First, a solution of fluorescent red (FR), cholecalciferol (CC), and octyltriethoxysilane (OTES) in ethanol was prepared. FR was selected as a typical example of a perylene-type dye. CC was used as an aliphatic, lipophilic molecule to dilute FR in the solid state and to disturb the π-stacking of the perylene molecules. In addition, CC – also known as vitamin D$_3$, which is produced in mammals by the skin when exposed to sunlight[12] – can be considered a biocompatible solvent. OTES serves as the starting material to form the SiO$_2$ shell *via* controlled hydrolysis of the ethoxy groups, and with the lipophilic octyl group to stabilise the lipophilic core of the aimed core@shell nanoparticles (Fig. 1). Moreover, ethanol allows a reduction of the viscosity of the solution as well as a fast mixing and reaction after the injection.

The solution of FR, CC, and OTES in ethanol was injected into water under vigorous stirring at slightly acidic conditions of pH 5 and a temperature of 70 °C (Fig. 1). With these conditions, the formation of FR/CC@SiO$_2$ core–shell nanoparticles can be rationalized as follows. First of all, ethanol was dissolved in the aqueous medium with the lipophilic FR and CC becoming insoluble in water. Due to the fast injection at elevated temperatures, fast particle nucleation occurs. During nucleation, moreover, the lipophilic octyl chains of OTES were
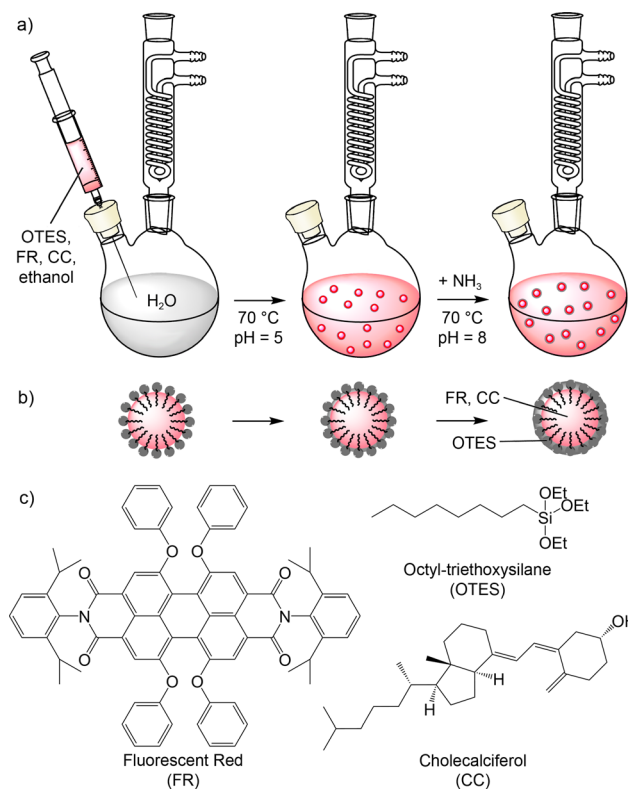

Fig. 1 Schematic illustration of the water-based injection-based synthesis of FR/CC@SiO$_2$ core–shell nanoparticles: (a) synthesis, (b) structure of nanoparticle, (c) structure of used molecules.

embedded in the as-formed FR/CC nanoparticles with the polar triethoxysilane group on the surface. The injection at elevated temperature and the presence of H$^+$ as a catalyst led to fast hydrolysis of the triethoxysilane groups and the formation of a silica network on the nanoparticle surface. Such a reaction is well-known for tetraethylorthosilicate (TEOS) and the so-called Stöber synthesis.[13] Prolonged heating at 80 °C results in completion of the hydrolysis of the ethoxy groups and the condensation of the resulting silanol groups to obtain a certain thickness of the silica network (Fig. 1). Finally, the pH of the suspension was adjusted to pH 8 by the addition of NH$_3$ to increase the charge stabilisation of the FR/CC@SiO$_2$ core–shell nanoparticles, and thus, to increase the colloidal stability of the suspensions.

The as-prepared aqueous FR/CC@SiO$_2$ nanoparticle suspensions are colloidally highly stable and do not show any sedimentation over several months even at concentrations up to 10 mg mL^{-1}. Suspensions as well as powder samples exhibit an intense red colour and show luminescence even with daylight. The intense fluorescence of aqueous suspensions as well as of powder samples already indicates a good luminescence efficiency and the absence of quenching even at high LR contents of 10 wt%. Finally, it should be noticed that an identical synthesis without CC resulted in nanoparticles with a clear red colour, indicating the presence of FR, but without any fluorescence. In the absence of CC, as expected, this finding can be ascribed to π-stacking of the perylene molecules resulting in a complete luminescence quenching.

This journal is © The Royal Society of Chemistry 2023

J. Mater. Chem. C, 2023, **11**, 616–621 | **617**

3.2 Characterisation of FR/CC@SiO₂ core–shell nanoparticles

The size, size distribution, and structure of the as-prepared FR/CC@SiO₂ core–shell nanoparticles were examined by dynamic light scattering (DLS) and electron microscopy (Fig. 2). DLS analysis of aqueous suspensions shows a mean hydrodynamic diameter of 35 ± 16 nm with a narrow size distribution (Fig. 2c). Scanning electron microscopy (SEM) shows a spherical shape and confirms a mean particle diameter of 29 ± 11 nm (Fig. 2a and c), which was calculated from the statistical evaluation of 150 nanoparticles on SEM images. Zeta potential measurements showed high negative surface charging of -40 to -50 mV at a pH range of 6–9 (Fig. 2d), which reflected the high colloidal stability of the as-prepared aqueous suspensions. In this context, suspensions are usually considered colloidally stable if the zeta potential is either below -30 mV or above $+30$ mV.[14] This allows to realise aqueous suspensions with particle concentrations up to 10 mg mL^{-1}, which are colloidally stable over several months, without the need for any additional stabiliser and surface functionalisation.

Scanning transmission electron microscopy (STEM) confirmed the presence of spherical nanoparticles, about 30 nm in diameter, and clearly pointed to the inner FR/CC-filled cavity (Fig. 2c). The cavity has a diameter of 12 ± 4 nm surrounded by a SiO₂ shell, 9 ± 4 nm in thickness. Here, it must be noticed that the FR/CC@SiO₂ core–shell nanoparticles start to decompose under the bombardment of high-energy electrons. For such fragile nanoparticles with a high load of organic material, often SEM (at acceleration voltages of 1–30 kV) is more advantageous for imaging (compare Fig. 2a and b) than TEM (with acceleration
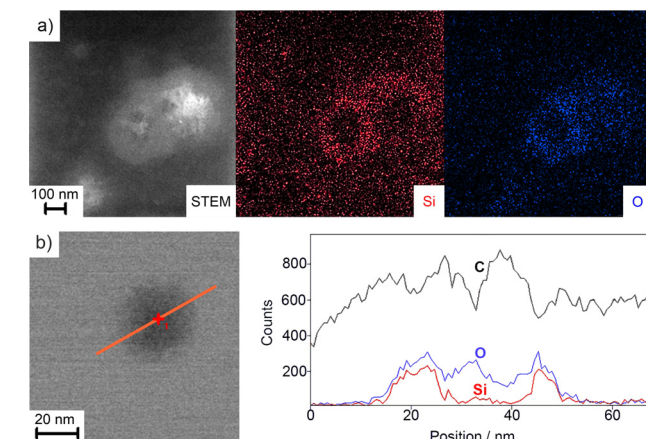
voltages of 80–300 kV).[15] To further examine the core@shell-type structure, energy-dispersive X-ray spectroscopy (EDXS) was performed (Fig. 3). EDXS area scans (Fig. 3a) and EDXS line scans (Fig. 3b) evidenced the core@shell-type structure with a SiO₂ shell and a carbon-rich inner cavity. Cavity diameter and wall thickness can again be deduced to 10–15 nm and 8–10 nm, respectively.

The amounts of FR and CC in the nanoparticle cavity were evaluated using Fourier-transformed infrared (FT-IR) spectroscopy, elemental analysis (EA), and X-ray powder diffraction (XRD) techniques. FT-IR shows vibrations of SiO₂ (ν(Si–O–Si): 1200–950, ν(Si–OH): 950–880, δ(Si–O–Si): 700–500 cm^{-1}), FR (fingerprint area: 100–500 cm^{-1}), CC (ν(C–H): 3000–2800, ν(C=C): 1635, ν(C–O): 1049, fingerprint area: 1480–650 cm^{-1}), as well as of water (ν(O–H): 3500–3000 cm^{-1}) (Fig. 4a). EA results in contents of 58.19% C, 9.37% H, 0.27% N, and a solid residue of 32.17%. The solid residue can be attributed to SiO₂. Since N is only present in FR, a total weight of 10.4 wt% FR per FR/CC@SiO₂ core–shell nanoparticle can be deduced. According to XRD, the FR/CC@SiO₂ core–shell nanoparticles, as expected, are non-crystalline (Fig. 4b). Two broad reflexes can be related to CC when compared to reference diffractograms. Interestingly, CC in the inner cavity of the nanoparticles is not crystalline.
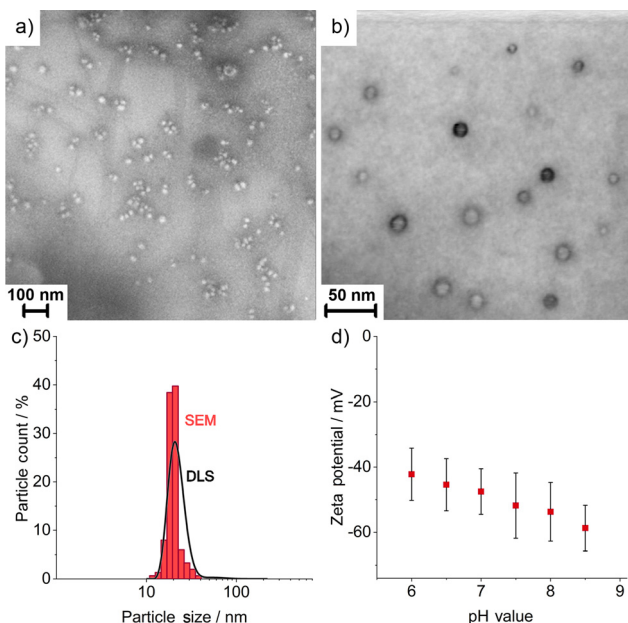

Fig. 3 Structure of FR/CC@SiO₂ core–shell nanoparticles: (a) EDXS area scans with element mapping and (b) EDXS line scan with concentration profile at the position of the orange line on the STEM image.

Fig. 2 Size, shape, and colloidal stability of FR/CC@SiO₂ core–shell nanoparticles: (a) particle size according to SEM overview images; (b) particle shape and inner cavity according to STEM detail image; (c) size distribution according to SEM and DLS; (d) zeta-potential of aqueous suspension at different pH values.
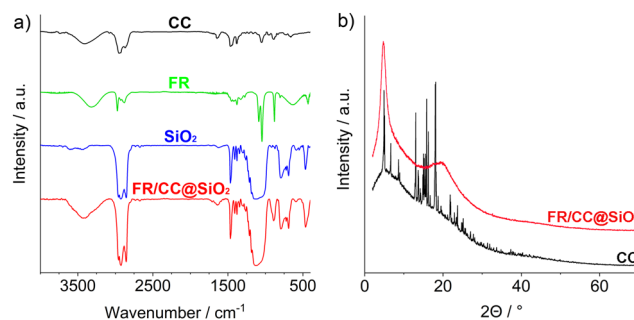

Fig. 4 Chemical composition of the as-prepared PR/CC@SiO₂ core–shell nanoparticles: (a) FT-IR spectra with FR, CC, and SiO₂ as a reference (SiO₂ prepared by hydrolysis of OTES); (b) XRD patterns with CC as a reference.

618 | J. Mater. Chem. C, 2023, **11**, 616–621

This journal is © The Royal Society of Chemistry 2023

Obviously, crystallization is disturbed by the presence of FR and OTES, which, *vice versa*, also disturbs the π-stacking of the perylene molecules.

3.3 Fluorescence of FR/CC@SiO$_2$ core–shell nanoparticles

To examine the luminescence properties of the FR/CC@SiO$_2$ core–shell nanoparticles, UV-Vis and photoluminescence (PL) spectroscopy were performed (Fig. 5). Upon comparison to reference spectra of FR, CC, and SiO$_2$, the optical absorption of the FR/CC@SiO$_2$ core–shell nanoparticles can be attributed to FR in the visible spectral range (350–700 nm) (Fig. 5a). The characteristic absorption of FR can be also used to quantify the FR content following the Lambert–Beer formalism (Fig. S2, ESI†). Accordingly, the FR content was 10.8 wt%, which is in good agreement with the amount determined *via* EA (10.4 wt%). At lower wavelengths, the absorption was dominated by CC (250–300 nm) and SiO$_2$ (especially ≤250 nm). According to PL spectra, excitation and emission of the FR/CC@SiO$_2$ core–shell nanoparticles were more-or-less identical to FR (Fig. 5b). Thus, excitation was observed at 400–500 nm; intense emission occurred at 480–750 nm. In comparison to FR/CC@SiO$_2$ core–shell nanoparticles, we also examined the absorption and photoluminescence of CC-free FR@SiO$_2$ core–shell nanoparticles.† Despite the identical FR-load (1 mg mL^{-1}), the FR/CC@SiO$_2$ core–shell nanoparticles showed a significantly higher absorption below 400 nm (Fig. S3, ESI†). Similarly, the excitation and emission of the FR/CC@SiO$_2$ core–shell nanoparticles were dramatically higher as compared to those in the CC-free FR@SiO$_2$ core–shell nanoparticles (Fig. S4, ESI†). In fact, the emission of the FR/CC@SiO$_2$ core–shell nanoparticles was more than 10 times higher. In sum, these optical data point to the importance of CC in order to avoid the π-stacking of the perylene-type dye.

The absolute quantum yield of the FR/CC@SiO$_2$ core–shell nanoparticles was determined following a method reported by Friend *et al.*[16] As a result, a quantum yield of 98% was determined, which is similar to that of the freely dissolved perylene dye (in ethanol). This finding also confirms that no concentration quenching occurred. Thus, π-stacking of the perylene dye was indeed efficiently avoided in the core–shell nanoparticles due to the presence of CC and OTES although FR was applied with a high load of 10 wt%. Thus, the perylene load per nanoparticle was significantly higher compared to that previously reported for nanoparticles (1 wt%).[9] There, the authors used phenyltriethoxysilane as a silica precursor, which, in view of an intense emission and high quantum yield is counterproductive since the phenyl groups of the silane promote π-stacking and concentration quenching of the perylene dye.

Besides intense emission and high quantum yield, the encapsulation of FR with CC in the inner cavity of SiO$_2$ nanoparticles optionally could also lead to good photostability. To evaluate this concern, UV-Vis spectra of the FR/CC@SiO$_2$ core–shell nanoparticles (aqueous suspension) and freely dissolved FR (in ethanol) with identical FR-load (2.5 µg mL^{-1}) were continuously exposed to excitation over 20 h (Fig. 6). For excitation, we selected 280 nm as the UV light and 567 nm as the wavelength of maximum absorption of FR. With these wavelengths, on the one hand, UV stability, and on the other hand, excitation stability were monitored. Although perylene-type dyes such as FR are known for very high photostability in comparison to the majority of organic-dye molecules, nevertheless, a certain decrease in absorption occurs, which starts after 8 h and increases continuously thereafter (Fig. 6). This decrease of absorption indicates photoinduced decomposition of the dye and it occured for excitation at 280 nm as well as 567 nm. The decomposition at higher photon energy (280 nm), as expected, is stronger than that at 567 nm and can be ascribed to the formation of reactive oxygen species (ROS).[17] At 567 nm, the photodegradation of FR is lower compared to 280 nm, but continuous exposure nevertheless leads to a recognizable degradation of the freely dissolved FR caused by intramolecular charge carriers.[18] In contrast to the freely dissolved dye, the FR absorption of the FR/CC@SiO$_2$ core–shell nanoparticles remained completely unaffected upon exposure to 280 nm and 567 nm, which points to an efficient photostablisation.

In addition to the detailed characterisation of the FR/CC@SiO$_2$ core–shell nanoparticles, FO and FY were used as perylene-type dyes similar to FR to obtain FO/CC@SiO$_2$ and FY/CC@SiO$_2$ core–shell nanoparticles. Again, 10 wt% of the respective PD were encapsulated. Already the colour of the aqueous suspensions indicated the presence of FO and FY in the nanoparticles,
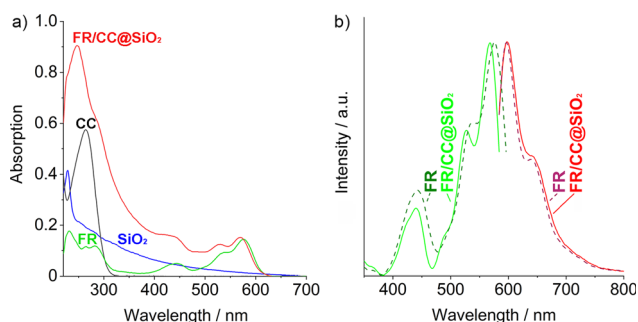

Fig. 5 Optical properties of the as-prepared FR/CC@SiO$_2$ core–shell nanoparticles (aqueous suspension): (a) UV-Vis spectrum with FR, CC, and SiO$_2$ as references; (b) excitation and emission spectra with freely dissolved FR as a reference (in ethanol, with emission monitored at λ_{em} = 600 nm and excitation recorded at λ_{exc} = 567 nm).
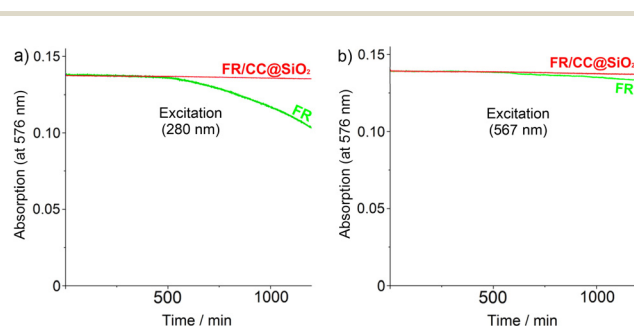

Fig. 6 Photostability of FR/CC@SiO$_2$ core–shell nanoparticles with continuous exposure for 20 hours at (a) 280 nm, (b) 567 nm (UV-Vis spectra recorded at 567 nm for both types of exposure; aqueus FR/CC@SiO$_2$ suspension and freely dissolved FR in ethanol with identical FR-load of 2.5 µg mL^{-1}).

This journal is © The Royal Society of Chemistry 2023

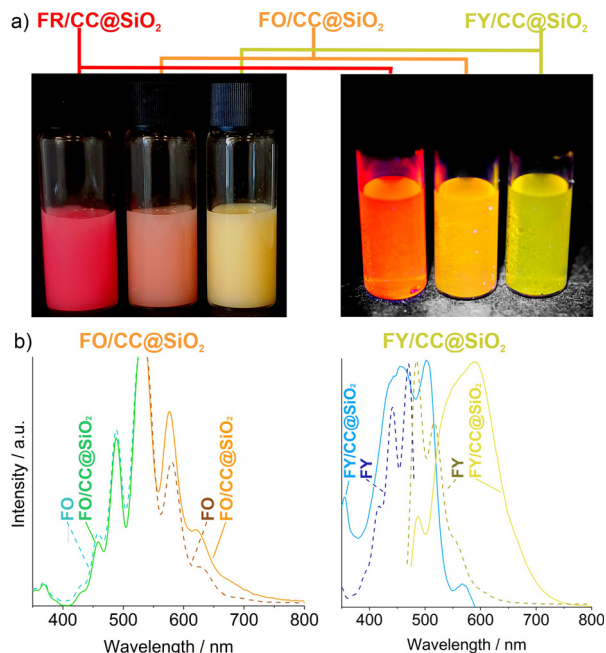*J. Mater. Chem. C*, 2023, **11**, 616–621 | **619**

Fig. 7 PD/CC@SiO$_2$ core–shell nanoparticles with FR, FO, and FY as fluorescent dyes: (a) photos of suspensions in daylight and with excitation (λ_{exc} = 366 nm), (b) excitation and emission spectra (in H$_2$O, with emission monitored at λ_{em} = 525 nm/FO, 460 nm/FY and excitation recorded at λ_{exc} = 550 nm/FO, 605 nm/FY).

which also showed intense fluorescence in daylight (Fig. 7a). The excitation and emission spectra of FR/CC@SiO$_2$ (Fig. 5b), FO/CC@SiO$_2$, and FY/CC@SiO$_2$ core–shell nanoparticles showed the shift of the emission from red to yellow (Fig. 7b). Mixing of two PDs inside the nanoparticles also gave the option to further shift the emission continuously between the ones of the pure perylene dyes.

As a proof-of-the-concept, finally, thin films of FR/CC@SiO$_2$ core–shell nanoparticles were prepared (Fig. 8). On the one hand, a pen was filled with FR/CC@SiO$_2$ core–shell nanoparticles as a water-based ink. The written text was invisible without excitation but clearly visible after excitation (Fig. 8a). Moreover, a few drops of an aqueous suspension (10 mg mL^{-1})

Fig. 8 Thin films with FR/CC@SiO$_2$ core–shell nanoparticles: (a) scheme of a pen filled with aqueous nanoparticle suspension and photos of written letters without and with excitation (λ_{exc} = 366 nm), (b) scheme of nanoparticles between two quartz-glass plates and photos in daylight and with excitation (λ_{exc} = 366 nm) (due to whitener the paper with the logo shows certain white emission itself).

were deposited on a quartz-glass plate (50 × 50 mm), and a second quartz-glass plate was pressed on top (Fig. 8b). After drying at room temperature, the ensemble was highly transparent and showed an intense red emission upon excitation (366 nm).

4. Conclusion

PD/CC@SiO$_2$ core–shell nanoparticles (PD: perylene dye, CC: cholecalciferol/vitamin D$_3$) were prepared by a water-based injection method. To this end, a solution of the PD fluorescent red (FR), fluorescent orange (FO), fluorescent yellow (FY), CC, and octyltriethoxysilane (OTES) as the silica precursor in ethanol were injected in water at pH 5 and 70 °C. The core–shell nanoparticles exhibited an outer particle diameter of 29 ± 11 nm and an inner cavity of 12 ± 4 nm. Suspensions (up to 10 mg mL^{-1}) were colloidally highly stable due to the negative surface charging (−40 to −50 mV). CC efficiently allowed disturbing of the π-stacking of the PD, such that FR/CC@SiO$_2$ nanoparticles showed intense emission with quantum yields of near unity (98%) and without concentration quenching even at high FR load (10 wt%). In contrast to the freely dissolved dyes, moreover, the PD in the nanoparticle core did not show any photobleaching even after 20 hours of continuous UV illumination (280 nm). As a proof-of-the-concept, suspension and thin films were realised showing intense emission from red to yellow. Exemplarily, FR/CC@SiO$_2$ core–shell nanoparticles were examined in detail, including electron microscopy, element mapping, dynamic light scattering, infrared spectroscopy, elemental analysis, UV-Vis, and photoluminescence spectroscopy.

Conflicts of interest

There are no conflicts to declare.

Acknowledgements

References

1 C. Huang, S. Barlow and S. R. Marder, *J. Org. Chem.*, 2011, **76**, 2386–2407.

2 D. K. Bhowmick, L. Stegemann, M. Bartsch, C. A. Strassert and H. Zacharias, *J. Phys. Chem. C*, 2016, **120**, 3275–3288.

3 B. Zhang, H. Soleimaninejad, D. J. Jones, J. M. White, K. P. Ghiggino, T. A. Smith and W. W. H. Wong, *Chem. Mater.*, 2017, **29**, 8395–8403.

4 J. P. Hoogenboom, E. M. H. P. Van Dijk, J. Hernando, N. F. van Hulst and M. F. García-Parajó, *Phys. Rev. Lett.*, 2005, **95**, 097401.

5 (*a*) K. Pal, V. Sharma, D. Sahoo, N. Kapuria and A. L. Koner, *Chem. Commun.*, 2018, **54**, 523–526; (*b*) K. Trofymchuk, A. Reisch, I. Shulov, Y. Mély and A. S. Klymchenko, *Nanoscale*, 2014, **6**, 12934–12942; (*c*) C. S. Fischer, M. C. Baier and S. Mecking, *J. Am. Chem. Soc.*, 2013, **135**, 1148–1154; (*d*) Q. Zhao, K. Li, S. Chen, A. Qin, D. Ding, S. Zhang, Y. Liu, B. Liu, J. Z. Sun and B. Z. Tang, *J. Mater. Chem.*, 2012, **22**, 15128–15135; (*e*) D. Zhuang and T. E. Hogen-Esch, *Macromolecules*, 2010, **43**, 8170–8176.

6 Z. Yang, W. Fan, J. Zou, W. Tang, L. Li, L. He, Z. Shen, Z. Wang, O. Jacobson, M. A. Aronova, P. Rong, J. Song, W. Wang and X. Chen, *J. Am. Chem. Soc.*, 2019, **141**, 14687–14698.

7 M. Fu, F. Ehrat, Y. Wang, K. Z. Milowska, C. Reckmeier, A. L. Rogach, J. K. Stolarczyk, A. S. Urban and J. Feldmann, *Nano Lett.*, 2015, **15**, 6030–6035.

8 (*a*) L. Zong, H. Zhang, Y. Li, Y. Gong, D. Li, J. Wang, Z. Wang, Y. Xie, M. Han, Q. Peng, X. Li, J. Dong, J. Qian, Q. Li and Z. Li, *ACS Nano*, 2018, **12**, 9532–9540; (*b*) Z. Yang, R. Tian, J. Wu, Q. Fan, B. C. Yung, G. Niu, O. Jacobson, Z. Wang, G. Liu, G. Yu, W. Huang, J. Song and X. Chen, *ACS Nano*, 2017, **11**, 4247–4255; (*c*) A. Jana, L. Bai, X. Li, H. Ågren and Y. Zhao, *ACS Appl. Mater. Interfaces*, 2016, **8**, 2336–2347.

9 F. Corsini, E. Tatsi, A. Colombo, C. Dragonetti, C. Botta, S. Turri and G. Griffini, *Nano Energy*, 2021, **80**, 105551.

10 E. H. Cho, M. S. Kim, D. H. Park, H. Jung, J. Bang, J. Kim and J. Joo, *Adv. Funct. Mater.*, 2011, **21**, 3056–3063.

11 C. de Mello Donegá, P. Liljeroth and D. Vanmaekelbergh, *Small*, 2005, **1**, 1152–1162.

12 P. Lips, *Prog. Biophys. Mol. Biol.*, 2006, **92**, 4–8.

13 N. J. Halas, *ACS Nano*, 2008, **2**, 179–183.

14 G. A. Parks, *Chem. Rev.*, 1965, **65**, 177–198.

15 S. Wolf and C. Feldmann, *Angew. Chem., Int. Ed.*, 2016, **55**, 15728–15752.

16 J. C. de Mello, H. F. Wittmann and R. H. Friend, *Adv. Mater.*, 1997, **9**, 230–232.

17 Q. Zheng, M. F. Juette, S. Jockusch, M. R. Wasserman, Z. Zhou, R. B. Altman and S. C. Blanchard, *Chem. Soc. Rev.*, 2014, **43**, 1044–1056.

18 E. M. S. Stennett, M. A. Ciuba and M. Levitus, *Chem. Soc. Rev.*, 2014, **43**, 1057–1075.

This journal is © The Royal Society of Chemistry 2023

J. Mater. Chem. C, 2023, **11**, 616–621 | **621**